Modifying Critical Exponents of Magnetic Phase Transitions via Nanoscale Materials Design

Lorenzo Fallarino,[1] Eva López Rojo,[1,2] Mikel Quintana,[1] Juan Sebastián Salcedo Gallo,[3] Brian J. Kirby,[4] and Andreas Berger[1]

[1]CIC nanoGUNE BRTA, E-20018 Donostia—San Sebastián, Spain
[2]Faculty of Science, University of Valladolid, E-47011 Valladolid, Spain
[3]Departamento de Física y Química, Universidad Nacional de Colombia, 170003 Manizales, Colombia
[4]NIST Center for Neutron Research, Gaithersburg, Maryland 20899, USA

(Received 29 January 2021; accepted 10 August 2021; published 28 September 2021)

We demonstrate a nanoscale materials design path that allows us to bypass universality in thin ferromagnetic films and enables us to tune the critical exponents of ferromagnetic phase transitions in a very wide parameter range, while at the same time preserving scaling in an extended phase space near the Curie temperature. Our detailed magnetometry results reveal that single crystal CoRu alloy films, in which the predefined depth dependent exchange coupling strength follows a V-shaped profile, exhibit critical scaling behavior over many orders of magnitude. Their critical exponents, however, can be designed and controlled by modifying their specific nanoscale structures, thus demonstrating full tunability of critical behavior. The reason for this tunability and the disappearance of universality is shown to be the competing relevance of collective versus interface propagating progression of ferromagnetic phase transitions, whose balance we find to be dependent on the specifics of the underlying exchange coupling strength profile.

DOI: 10.1103/PhysRevLett.127.147201

The paramagnetic (PM) to ferromagnetic (FM) phase transition at a sample specific Curie temperature T_C is one of the best-known examples of spontaneous symmetry breaking. Its scientific exploration has been instrumental for the derivation of theories, which successfully revealed that the observable critical behavior is solely dependent on the dimensionality of both the system and the order parameter [1–3]. Accordingly, $Y_3Fe_5O_{12}$ [4], $La_{0.7}Sr_{0.3}MnO_3$ [5], and Ni [6], for instance, exhibit a single set of critical exponents associated with their symmetry class despite having different material characteristics, including the specific exchange interaction mechanism causing their ferromagnetic ground state. Most relevantly, universality enabled the description of rather complex physical systems by means of simple models, in particular local spin models, and still derive quantitatively accurate information about their phase transitions [7–8]. On the flip side of this enormous scientific success of achieving a unified description of phase transitions, universality implied that the PM-FM phase transition and associated critical exponents cannot be relevantly impacted by materials design as opposed to T_C values, for instance, which do depend on microscopic details. This in turn severely limits materials design capabilities towards the onset of FM order.

The only seeming exception to universality are phase transitions at surfaces of three-dimensional (3D) systems with Ising model character [9–10], for which the surface critical exponent β_S of the magnetization can be changed by modifying the surface exchange coupling strength J_S relative to its bulk counterpart J_{bulk} [11]. However, this strategy is very limited in its utility since only few individual β_S values are possible, namely, $\beta_S \approx 0.125$ for $J_S/J_{\text{bulk}} > 1.55$ and $\beta_S \approx 0.78$ for $J_S/J_{\text{bulk}} < 1.55$ [11]. They are furthermore very difficult to access, given that J_S tuning in a single atomic layer cannot be easily achieved in real materials [12]. Also, universality is not truly broken, because at the critical J_S threshold, the dimensionality of the magnetic state changes from a 3D surface state for $J_S/J_{\text{bulk}} < 1.55$ to a 2D thin film state for $J_S/J_{\text{bulk}} > 1.55$.

Therefore, it is not clear whether universality of PM-FM phase transitions can be circumvented by means of adapted materials design and it is this very question that we are addressing here. For this purpose, we devised a material design with a nanoscale V-shaped J depth profile, as depicted in Fig. 1(a). The ferromagnetic state is expected to form at T_C initially in the sample center [13–15], i.e., near $z = 0$. This generates a rather localized magnetization profile [16,17], which can be considered as a generalized version of the above-mentioned surface phase transition scenario. As we will demonstrate, such predefined depth modifications of J allow for the generation of tunable critical exponents β in a very wide parameter range and therefore circumvent universality.

To explore the case of V-shaped exchange strength gradients, we chose $Co_{1-x}Ru_x$ alloy layers as a model system, since their magnetic properties can be easily tuned by changing x [18–22]. A modification of J along the thickness z is achieved by varying the Ru content during the

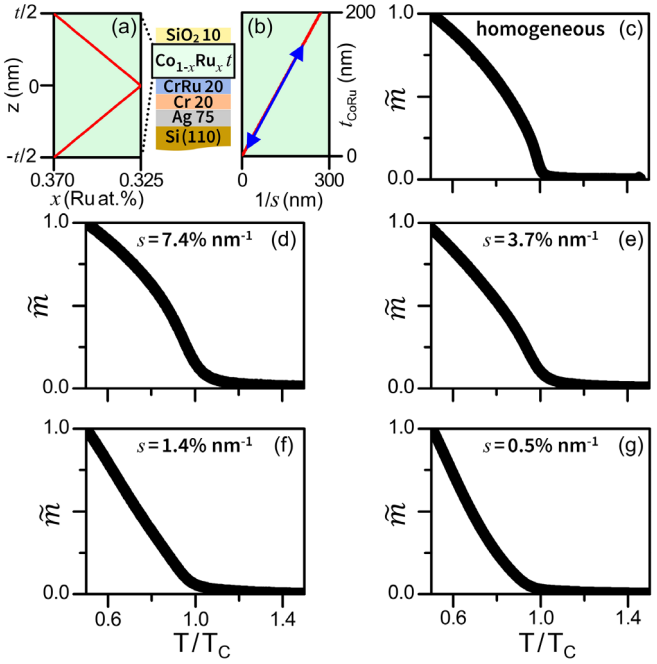

FIG. 1. (a) Depth profile of Ru content for our CoRu graded film samples, which are part of an overall layer growth sequence to facilitate epitaxy (layer thickness in nm); (b) linear relationship between t and $1/s$, which reflects our experimental strategy. The (blue) double arrow indicates the $(1/s, t)$ range explored in this work. (c)–(g) Temperature dependence of the normalized easy-axis magnetization $\tilde{m} = M/M(T/T_C = 0.5)$ for a $Co_{0.675}Ru_{0.325}$ homogeneous film (c), and graded structures for $s = 7.4\%$ (d), 3.7% (e), 1.4% (f), and 0.5% nm^{-1} (g). The data were measured while cooling each sample from $T = 300$ to $T = 50$ K in the presence of an applied field $\mu_0 H = 4$ mT.

growth. The resulting $Co_{1-x(z)}Ru_{x(z)}$ modulation scheme is shown on Fig. 1(a), with $x(z)$ varying linearly from $x_{max} = 0.37$ at the bottom and top to $x_{min} = 0.325$ at the center, which translates into a J profile that is described by

$$J(z) = J_0[1 - (s|z|)^{\phi}], \tag{1}$$

with J_0 being the maximum value in the center ($z = 0$) and $\phi = 1$. The slope $s > 0$ of the J profiles is defined as $(1\text{-}T_C^{min}/T_C^{max})/(t/2)$, with $10 \le t \le 150$ nm being the thickness of the CoRu layer, and T_C^{min} and T_C^{max} being the T_C values of homogeneous $Co_{0.63}Ru_{0.37}$ and $Co_{0.675}Ru_{0.325}$ reference samples, respectively. Since T_C is proportional to J for uniform magnetic systems, s determines the rate at which J varies along the z axis. Its values are quantified as the J reduction (in percent of J_0) per nm [21]. The absolute difference between x_{max} and x_{min} and consequently the ratio T_C^{min}/T_C^{max} are kept fixed in our experiments to ensure that the samples and measurements were performed under stable conditions. The corresponding experimental strategy is shown in Fig. 1(b), in which our sample series represents a line in the $(t, 1/s)$ plane with the (blue) arrows indicating the here explored t-s range. Moreover, to ensure that only a depth dependence of the magnetization occurs in our graded magnetic films, all samples are grown epitaxially, following the layer sequence shown in Fig. 1(a), so that they exhibit uniaxial magnetocrystalline anisotropy with the easy axis (EA) of magnetization oriented in the film plane. This suppresses the magnetostatic energy and leads to a lateral magnetic behavior that is very accurately described by a macrospin model [22–24]. For comparison purposes, homogeneous $Co_{1-x}Ru_x$ ($x = 0.325$, 0.347, 0.37) samples were fabricated using an identical underlayer sequence. X-ray diffraction measurements confirmed the epitaxial nature of all samples [24], while magnetometry data verified the in-plane uniaxial anisotropy, with the magnetization vector being homogeneous within each plane and collinear everywhere [23,24].

The M vs T behavior was measured from $T = 300$ K down to $T = 50$ K for all samples in the presence of an in-plane magnetic field, which was applied along the EA to select only one of the two possible ferromagnetic states in our uniaxial samples. The field magnitude was kept small to avoid the magnetization onset to be smeared out substantially [24]. Exemplary datasets are plotted in Figs. 1(c)–1(g). For a side-by-side visual comparison, the magnetization is normalized to its respective value at $T = 0.5T_C$. The resulting temperature dependence for a homogeneous sample, displayed in Fig. 1(c), shows the expected sharp magnetization onset at T_C. Similar characteristics are found in the graded structure with the largest s value, Fig. 1(d), even though M and J depth profiles are both present in this sample. This suggests that the resulting magnetic state along the depth of the film is strongly correlated, just as in conventional magnetic films. The effect of materials design by means of J grading becomes increasingly significant upon decreasing s [Figs. 1(e)–1(g)], where the phase transition exhibits first a weaker curvature for $s = 3.7\%$ nm^{-1}, becomes almost linear for $s = 1.4\%$ nm^{-1}, and finally even acquires a convex characteristic for $s = 0.5\%$ nm^{-1}.

To provide an accurate quantitative analysis of the critical behavior, a scaling approach based on the Arrott-Noakes equation of state [25] was applied to $M(T, H)$ datasets for different s. Typically, to determine the critical exponents by means of such a scaling approach, magnetic isotherms are measured in evenly spaced temperature steps and in a temperature range close to the critical temperature. However, it is fundamentally equivalent and practically easier to achieve an improved temperature resolution, if one measures a series of $M(T)$ curves for different applied field strengths, which we have done for four applied field values, namely, $\mu_0 H = 4$, 5, 10, 20 mT. For each sample we fit simultaneously four $M(T)$ curves in the temperature range $-0.2 < \tau = (T/T_C - 1) < 0.2$ to the scaling relation:

$$\left(\frac{H}{M}\right)^{\frac{1}{\gamma}} = \frac{T - T_C}{T_1} + \left(\frac{M}{M_1}\right)^{\frac{1}{\beta}}. \quad (2)$$

Hereby, the critical exponents β and γ, T_C, and the scaling factors M_1 and T_1 were utilized as fit parameters. Figures 2(a)–2(e) show the excellent agreement between the least-squares fitting results (red solid lines) and the data for the $Co_{0.675}Ru_{0.325}$ homogeneous sample (a), and for exemplary cases of graded samples representing $s = 7.4\%$ (b), 2.5% (c), 1.2% (d), and 0.5% nm^{-1} (e) [24]. The validity of this approach has been verified by the scaling plots in Figs. 2(f)–2(j), in which the scaled magnetization $M/|\tau|^{\beta}$ is plotted as a function of the scaled magnetic field $\mu_0 H/|\tau|^{\beta+\gamma}$. Figure 2(f) shows the results for the $Co_{0.675}Ru_{0.325}$ homogeneous sample. Excellent scaling is observed over at least 5 orders of magnitude in the renormalized field within the critical temperature range by displaying a collapse of all data onto two independent branches, one for the ferromagnetic ($T < T_C$) and one for the paramagnetic ($T > T_C$) state. Likewise, the resulting plots for the graded systems [Figs. 2(g)–2(j)] demonstrate excellent scaling, which is preserved in a wide parameter range in the vicinity of T_C using a single value for the critical exponents in each sample. This alone is a nontrivial observation, since it was *a priori* not clear whether systems that encompass complex magnetization profiles, which contain internal PM-FM quasi-interfaces [13,16,17,23], could still be represented by a single set of critical exponents over an extended temperature and phase space region. For the two extremes cases we find that β ($s = 7.4\%$ nm^{-1}) is very close to the value for the homogeneous sample, whereas β ($s = 0.5\%$ nm^{-1}) is far larger and even far larger than the expected value for the surface phase transition of a 3D system.

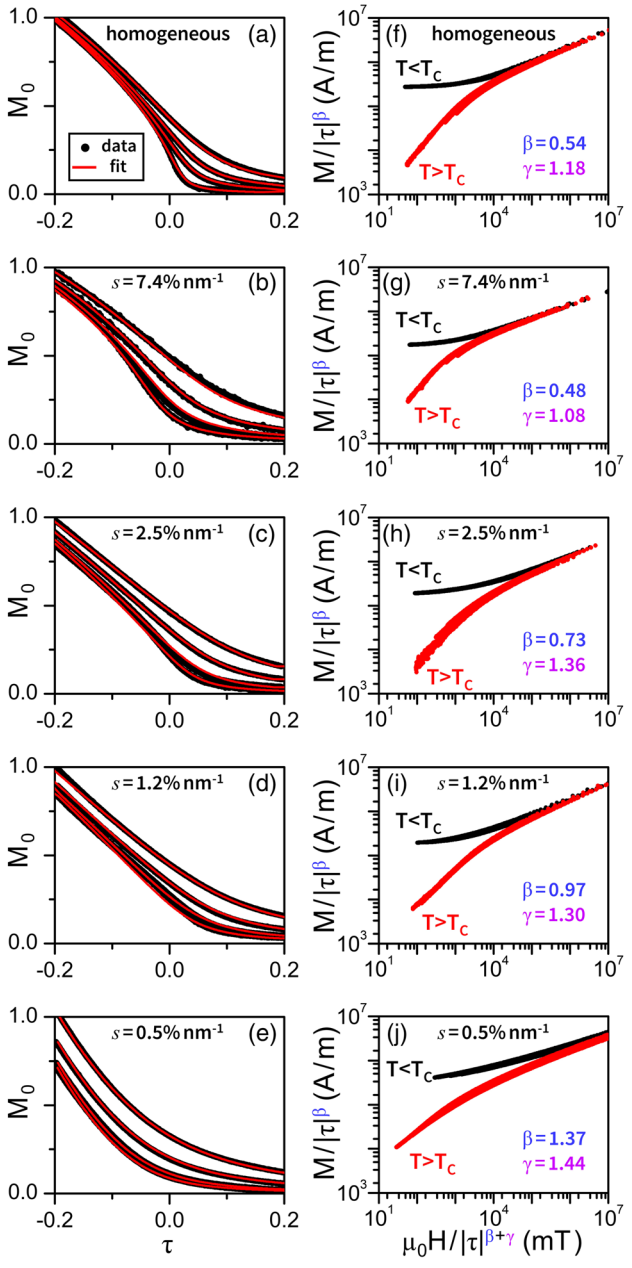

FIG. 2. (a)–(e) Temperature dependence of the normalized easy-axis magnetization $M_0 = M/M(\tau = T/T_C - 1 = -0.2)$ measured for four different magnetic field strengths $\mu_0 H = 4$, 5, 10, 20 mT for a $Co_{0.675}Ru_{0.325}$ homogeneous (a), and graded films with $s = 7.4\%$ (b), 2.5% (c), 1.2% (d), and 0.5% nm^{-1} (e). The (red) lines show least-squares fit to Eq. (2). (f)–(j) scaling plots of the easy-axis magnetization for the same homogeneous (f) and graded films (g)–(j).

The entire set of extracted β values, together with their estimated confidence intervals, are plotted in Fig. 3(a) as a function of $1/s$, along with the critical exponents for homogeneous systems, their average value β_{hom}, and $\beta_{\text{hom}} + 1$. The corresponding R^2 coefficients of the multi-field fitting are displayed as (red) triangles, showing values better than $R^2 > 0.995$ values in all cases [24]. The values of β, however, are very different depending on the specific gradient structure, covering an extremely broad range from the bulk system value β_{hom} for large s to asymptotically approaching $\beta_{\text{hom}} + 1$ upon decreasing s, seemingly violating universality. In contrast to β, the values of γ are rather constant and show only a modest systematic increase with $1/s$ [24]. To properly interpret Fig. 3(a), one has to keep in mind that in our study $\Delta J = J_0 - J_{\text{min}}$ is constant, and thus a variation of s is always associated with a change in t as well, as illustrated in Fig. 1(b). Thus, if one chooses ΔJ differently, the exact numerical values for β vs $1/s$ change, given that they now correspond to different t values [24]. However, the association of β with s is the most meaningful, because without any gradient structure, the observed anomalous critical behavior would not occur. To properly understand the underlying physics of the evaluated β values, one should consider how the material orders magnetically in the vicinity of its T_C. As the samples have a V-shaped depth profile with the largest J in its center, the ferromagnetic state at T_C forms in the samples center

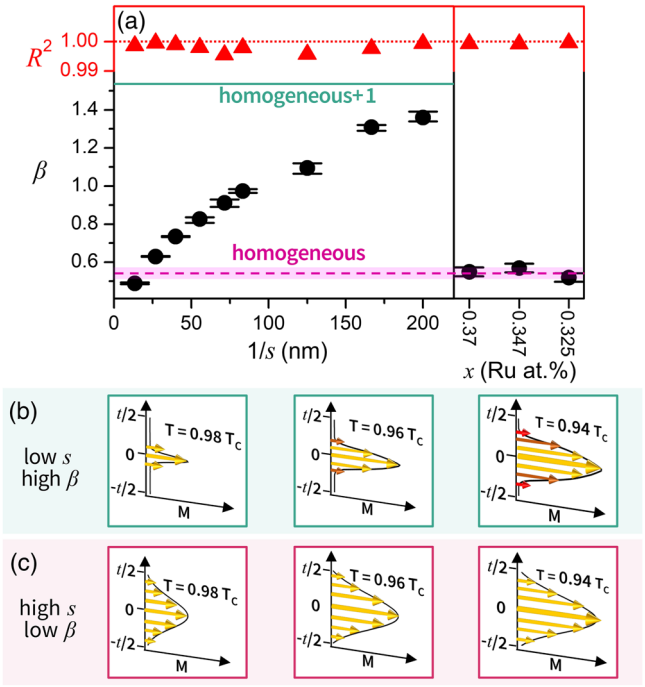

FIG. 3. (a) $1/s$ dependence of the extracted critical exponent β (black circles) together with the confidence interval of each least-square fit, shown as error bars [25], and the corresponding R^2 coefficients (red triangles). The dotted (red) line displays $R^2 = 1$. The (pink) dashed line indicates the average measured β value (the highlighted region corresponds ± 1 standard deviation) for the homogeneous systems investigated in this work, shown on the right side of (a), while the solid (green) line indicates this value $+1$. (b) and (c) Schematics of the temperature evolution of the magnetization depth profile for a system with low-s and high-s values, respectively.

first [13,16]. Hereby, it will not be limited to the central layer only but will result in a broadened magnetization structure on the nm scale, since the central layer induces a nonvanishing magnetization into adjacent layers via interlayer exchange coupling [16,17]. However, the induced magnetization falls off exponentially in the top and bottom segments, so that the ferromagnetically ordered film thickness is considerably smaller than the total thickness for small s and correspondingly large t samples, as depicted in Fig. 3(b). If the temperature is now lowered, the magnetization in the central profile region increases its magnitude and at the same time widens its profile [16]. This occurs because the ferromagnetic state becomes stable over an ever-larger segment of the film, as shown by the schematics for $T = 0.96T_C$ and $0.94T_C$ and highlighted by the dark (red) arrows. Thus, upon lowering the temperature, the magnetic profile is extending further and further into the 3rd dimension of the film, but its width stays smaller than the film thickness for a significant temperature range. As a result, the critical exponent becomes a combination of the one representing the homogeneous system and the power law that describes the J-depth structure, specifically near its center, where the phase transition first materializes. In contrast, for high s samples, the 3rd dimension is already relevantly populated at T_C, as depicted in Fig. 3(c), since for such large gradients the total thickness t is comparable to the internal magnetic profile width at the first occurrence of ferromagnetic order. Therefore, a collective ferromagnetic behavior develops in the entire film, showing a conventional critical exponent with the magnetization increasing its magnitude but not its spatial extent upon lowering the temperature.

To advance our understanding of this behavior, we calculated the limiting β behavior for small s systems following a J profile according to Eq. (1) and arbitrary ϕ [24]. Given that in the low s case, the magnetic profile transition width in the vicinity of internal PM-FM quasi-interfaces is small compared to the length scale of the film itself, we can utilize a purely local phase transition scenario, in which a "local" Curie temperature is proportional to the local exchange coupling constant, so that

$$m(z,T) = D[T_C - T_C(s|z|)^{\phi} - T]^{\beta_{hom}} \quad \text{for } T < T_C[1-(s|z|)^{\phi}], \tag{3}$$

$$m(z,T) = 0 \quad \text{for } T \geq T_C[1-(s|z|)^{\phi}], \tag{4}$$

with D being a material specific constant and T_C being the dimensionless global Curie temperature [21], which is proportional to J_0. Utilizing Eq. (3) and (4), we calculate the sample magnetization $M(T)$ by averaging $m(z,T)$ over z. For $T \geq T_C$, $M(T) = 0$, given that no part of the sample has yet transitioned to the ferromagnetic state. For $T < T_C$, however, a fraction of the sample has become ferromagnetic, namely, the portion $-[(T_C - T)/T_C s^{\phi}]^{1/\phi} \leq z \leq [(T_C - T)/T_C s^{\phi}]^{1/\phi}$. Correspondingly, for $T < T_C$ we find

$$M(T) = \frac{2}{t}\int_0^{\left(\frac{(T_C-T)}{T_C s^{\phi}}\right)^{1/\phi}} dz\{D[T_C - T_C(s|z|)^{\phi} - T]^{\beta_{hom}}\}, \tag{5}$$

which can be rewritten, by using the hypergeometric function $\tilde{f}$ that has values of the order of 1 in the interval [0,1] for positive $\beta_{\mathrm{hom}} < 1$ [24], so that

$$M(T) = \frac{2D\tilde{f}}{tsT_C^{(1/\phi)}}(T_C - T)^{\beta_{\mathrm{hom}}+1/\phi} \quad \text{for } T < T_C, \tag{6}$$

$$M(T) = 0 \quad \text{for } T \geq T_C, \tag{7}$$

with the temperature dependence of the sample magnetization $M(T)$ exhibiting the anomalous critical exponent $\beta = (\beta_{\mathrm{hom}} + 1/\phi)$ for $s \to 0$, so that $\beta = \beta_{\mathrm{hom}} + 1$ in the $s \to 0$ limit for our experimental case. For very flat profiles in the center of such films, which are characterized by a very high ϕ, β approaches its homogeneous value, which is the appropriate limiting behavior [26]. Thus, the local

superposition model [24] explains the limiting behavior for $s \to 0$ and it aids our understanding of the anomalous critical β values for this limit as being driven by the synchronous magnetization profile growth in height and width. As such, it illustrates the underlying physics, but it does not aim at providing a full theoretical description for all s values. Therefore, our calculations by themselves do not prove that any intermediate s-value system would be well described by a single critical exponent. However, our experimental data [Figs. 2 and 3(a)] demonstrate that a single intermediate β-value properly characterizes the measured behavior while a theoretical verification of this fact is beyond the scope of this work.

In summary, we demonstrate a nanoscale materials design path towards the tuning of $M(T)$ critical behavior and exponent β with a large degree of freedom, namely, from β_{hom} to $\beta_{\mathrm{hom}} + 1$, while preserving critical scaling near T_C. Correspondingly, we observe that such nanoscale designed materials can bypass the universality of continuous phase transition, and instead make β a quantity that can be tuned in an extremely wide range upon altering the nanoscale materials design. We achieved this $M(T)$ tunability for a single ferromagnetic nanoscale material, which we accomplished to fabricate in single crystal form. This makes our approach not comparable to a simplistic macroscopic mixing of different ferromagnets, which can also modify the $M(T)$ dependence but only on a macroscopic ensemble average rather than within one ferromagnetic nanoscale entity. Given the generality of our observations and calculations, we expect that our findings will extend to different magnetic material systems [27–29]. Finally, our innovative concept, combining standard magnetic materials with predefined compositional architectures, offers a broadly available platform to promote nanoscale-based designs for the purpose of critical behavior management. Such an approach could be used to realize performance advances in a wide variety of applications that rely on thermally assisted processes [30–34], which to date are all lacking this capability.

We acknowledge financial support by the Spanish Ministry of Science and Innovation under the Maria de Maeztu Units of Excellence Program (MDM-2016-0618), the Project No. RTI2018-094881-B-100 and the Ph.D. fellowship No. PRE2019-088428. J. S. S. G. acknowledges the Colombian Ministry of Science, Technology and Innovation (MINCIENCIAS, Grant No. 812).

[1] H. E. Stanley, *Introduction to Phase Transitions and Critical Phenomena* (Clarendon Press, Oxford, 1971).
[2] C. Domb and M. S. Green, *Phase Transitions and Critical Phenomena* (Academic Press, New York, 1972), Vols. 1–6; C. Domb and J. Lebowitz, *Phase Transitions and Critical Phenomena* (Academic Press, New York, 1973–2001), Vols. 7–20.
[3] N. D. Goldenfeld, *Lectures on Phase Transitions and the Renormalization Group* (Addison-Wesley, Reading, MA, 1992).
[4] K. Miyatani and K. Yoshikawa, J. Appl. Phys. **41**, 1272 (1970).
[5] K. Ghosh, C. J. Lobb, R. L. Greene, S. G. Karabashev, D. A. Shulyatev, A. A. Arsenov, and Y. Mukovskii, Phys. Rev. Lett. **81**, 4740 (1998).
[6] L. P. Kadanoff, W. Götze, D. Hamblen, R. Hecht, E. A. S. Lewis, V. V. Palciauskas, M. Rayl, J. Swift, D. Aspnes, and J. Kane, Rev. Mod. Phys. **39**, 395 (1967).
[7] C. H. Back, Ch. Würsch, A. Vaterlaus, U. Ramsperger, U. Maier, and D. Pescia, Nature (London) **378**, 597 (1995).
[8] Z. Fei, B. Huang, P. Malinowski, W. Wang, T. Song, J. Sanchez, W. Yao, D. Xiao, X. Zhu, A. F. May, W. Wu, D. H. Cobden, J.-H. Chu, and X. Xu, Nat. Mater. **17**, 778 (2018).
[9] K. Binder and P. C. Hohenberg, Phys. Rev. B **6**, 3461 (1972).
[10] K. Binder and P. C. Hohenberg, Phys. Rev. B **9**, 2194 (1974).
[11] K. Binder and D. P. Landau, Phys. Rev. Lett. **52**, 318 (1984).
[12] S. Langridge, G. M. Watson, D. Gibbs, J. J. Betouras, N. I. Gidopoulos, F. Pollmann, M. W. Long, C. Vettier, and G. H. Lander, Phys. Rev. Lett. **112**, 167201 (2014).
[13] B. J. Kirby, H. F. Belliveau, D. D. Belyea, P. A. Kienzle, A. J. Grutter, P. Riego, A. Berger, and C. W. Miller, Phys. Rev. Lett. **116**, 047203 (2016).
[14] C. LeGraët, T. R. Charlton, M. McLaren, M. Loving, S. A. Morley, C. J. Kinane, R. M. D. Brydson, L. H. Lewis, S. Langridge, and C. H. Marrows, APL Mater. **3**, 041802 (2015).
[15] M. Marcellini, M. Pärnaste, B. Hjörvarsson, and M. Wolff, Phys. Rev. B **79**, 144426 (2009).
[16] B. J. Kirby, L. Fallarino, P. Riego, B. B. Maranville, C. W. Miller, and A. Berger, Phys. Rev. B **98**, 064404 (2018).
[17] L. Fallarino, P. Riego, B. J. Kirby, C. W. Miller, and A. Berger, Materials **11**, 251 (2018).
[18] V. Pierron-Bohnes, N. Ringelstein, A. Michel, S. Boukari, L. Bouzidi, N. Persat, E. Beaurepaire, M. Hehn, D. Muller, and M. C. Cadeville, J. Magn. Magn. Mater. **165**, 176 (1997).
[19] S. B. Qadri, T. M. Keller, M. Laskoski, C. A. Little, and M. S. Osofsky, Appl. Phys. Lett. **91**, 214101 (2007).
[20] P. Riego, L. Fallarino, C. Martínez-Oliver, and A. Berger, Phys. Rev. B **102**, 174436 (2020).
[21] J. S. Salcedo-Gallo, L. Fallarino, J. D. Alzate-Cardona, E. Restrepo-Parra, and A. Berger, Phys. Rev. B **103**, 094440 (2021).
[22] O. Idigoras, U. Palomares, A. K. Suszka, L. Fallarino, and A. Berger, Appl. Phys. Lett. **103**, 102410 (2013).
[23] L. Fallarino, B. J. Kirby, M. Pancaldi, P. Riego, A. L. Balk, C. W. Miller, P. Vavassori, and A. Berger, Phys. Rev. B **95**, 134445 (2017).
[24] See Supplemental Material at http://link.aps.org/supplemental/10.1103/PhysRevLett.127.147201 for more details, which includes Refs. [3,16,17,22,25,26].
[25] A. Arrott and J. E. Noakes, Phys. Rev. Lett. **19**, 786 (1967).
[26] D. Belitz, T. R. Kirkpatrick, and R. Saha, Phys. Rev. Lett. **99**, 147203 (2007).
[27] R. K. Dumas, Y. Fang, B. J. Kirby, C. Zha, V. Bonanni, J. Nogues, and J. Åkerman, Phys. Rev. B **84**, 054434 (2011).

[28] A. F. Kravets, A. N. Timoshevskii, B. Z. Yanchitsky, M. A. Bergmann, J. Buhler, S. Andersson, and V. Korenivski, Phys. Rev. B **86**, 214413 (2012).
[29] L. Fallarino, B. J. Kirby, and E. E. Fullerton, J. Phys. D **54**, 303002 (2021).
[30] D. Weller, G. Parker, O. Mosendz, E. Champion, B. Stipe, X. Wang, T. Klemmer, G. Ju, and A. Ajan, IEEE Trans. Magn. **50**, 1 (2014).
[31] I. L. Prejbeanu, M. Kerekes, R. C. Sousa, H. Sibuet, O. Redon, B. Dieny, and J. P. Nozières, J. Phys. Condens. Matter **19**, 165218 (2007).
[32] X. Moya, S. Kar-Narayan, and N. D. Mathur, Nat. Mater. **13**, 439 (2014).
[33] M. Hudl, M. d'Aquino, M. Pancaldi, S.-H. Yang, M. G. Samant, S. S. P. Parkin, H. A. Dürr, C. Serpico, M. C. Hoffmann, and S. Bonetti, Phys. Rev. Lett. **123**, 197204 (2019).
[34] S. Mangin, M. Gottwald, C. H. Lambert, D. Steil, V. Uhlíř, L. Pang, M. Hehn, S. Alebrand, M. Cinchetti, G. Malinowski, Y. Fainman, M. Aeschlimann, and E. E. Fullerton, Nat. Mater. **13**, 286 (2014).